ELSEVIER

Journal of Power Sources 65 (1997) 133–141

JOURNAL OF POWER SOURCES

21

Bipolar lithium-ion battery development

Richard A. Marsh [a,*], Philip G. Russell [b], Thomas B. Reddy [b]

[a] *Wright Laboratory, Wright Patterson AFB, OH 45433-6503, USA*

[b] *Yardney Technical Products, Inc., 82 Mechanic Street, Pawcatuck, CT 06379, USA*

Received 23 October 1996; accepted 20 November 1996

Abstract

The bipolar battery design minimizes *IR* losses between adjacent cells in a cell-stack and provides for uniform current and potential distributions over the active surface area of each cell component. The rechargeable lithium-ion electrochemistry is capable of high pulse power for cell components arranged in bipolar configuration. This system has delivered more than 3000 charge discharge cycles of pulse power and five-second pulses at current densities as high as 70 mA cm^{-2}. The present programme is concerned with bipolar cell design, component fabrication and evaluation, multi-cell stack assembly and evaluation for development of a 270 V 2 Ah bipolar lithium-ion battery for aerospace and aircraft applications.

Keywords: Lithium-ion secondary batteries; Bipolar electrodes; Applications/aerospace

1. Introduction

The rechargeable lithium-ion electrochemistry has received considerable attention for the development of small coin, cylindrical and prismatic cell configurations for commercial electronic applications. The use of carbon materials as anodes to replace metallic lithium provides excellent cycling efficiency and improved safety characteristics to the system. The lithium-ion electrochemistry is a moderate rate system at best due to the nature of the intercalation–deintercalation processes in the non-metallic electrode components and to the use of aprotic organic electrolytes with relatively low conductivity values ($\sim 10^{-3}$ S cm^{-1}). The rate capability of a battery system can be improved through careful selection and matching of cell components and/or by making improvements in the battery design. In an attempt to improve the lithium-ion rate capability, this electrochemistry is being examined in a bipolar design, which minimizes *IR* type loss between adjacent cells in a cell-stack and provides for uniform current and potential distributions over the active surface area of each cell component. The present programme is concerned with bipolar cell design, component fabrication and evaluation, multi-cell stack assembly and evaluation for the development of a 270 V, 2 Ah bipolar lithium-ion battery for aerospace and aircraft applications.

* Corresponding author.

PII S0378-7753(96)02615-8

2. Experimental

2.1. Electrolyte preparation

All electrolytes were prepared in the R&D dry room under low humidity (<2% r.h. at 20°C) conditions. One molar solutions of $LiClO_4$, (Alfa, >99.9%) and $LiPF_6$ (Haslilmoto Chemicals, Japan, purity 99.9%) were prepared in a mixture (1:2 vol./vol.) of ethylene carbonate (Ferro Corporation, purity 99.9%) with dimethyl carbonate (Ferro Corporation, purity 99.98%), diethyl carbonate (Fluka, 99.5%) or dimethoxyethane (Aldrich, 99.9%). $LiPF_6$ was used as received. The $LiClO_4$ lithium salt was dried at 110°C under vacuum for a minimum of 48 h to lower its water content to less than 150 ppm prior to use. One molar solutions of $LiAsF_6$ (FMC) were prepared with 1:2 EC:DMC and EC:MF (methyl formate) mixed solvents. The water content of each electrolyte was determined with a Karl Fischer coulometer. All electrolytes were stored with lithium chips for at least 48 h under dry room conditions prior to cell activation.

2.2. Preparation of samples for chemical stability

Samples for the chemical compatibility study at 25, 40 and 60°C were prepared by mixing 10 ml of an electrolyte with 10 g of a lithiated metal oxide. Each sample mixture was contained in a screw-capped polypropylene bottle and stored for 1 week at one of the above temperatures. A fresh sample

of each electrolyte/oxide type was prepared for each of the above storage temperatures. Each sample was checked periodically for changes in electrolyte appearance. A 1 ml sample of 'filtered' electrolyte was submitted for DCP analysis of the appropriate transition metal after the 1 week storage period.

2.3. Electrode fabrication methods

The anode active carbon was petroleum coke (Conoco) or graphite (Lonza). The active carbon material was mixed with 10% PVDF (Aldrich) or Kynar® 2822 (Elf Atochem) binder dissolved in dimethyl formamide (DMF) to form the anode spray composition. The anode was prepared by spray-coating this composition onto the anode copper substrate. The cathode spray composition was prepared from a mixture of $LiCoO_2$ (Sherritt) or $LiNiO_2$ (FMC) lithiated metal oxide, a carbon black/graphite mixture and binder dissolved in DMF. The cathode was fabricated by spray-coating this composition onto the cathode aluminum substrate. The anode and cathode compositions were compressed to the desired density and thickness.

Self-supporting anodes and cathodes were prepared by spray-coating Whatman PD075 filter paper on one side with electrode composition, compressing the sprayed filter paper initially to 9 tonnes (20 000 lb) so that the paper backing layer could be easily removed and then compressing the electrode component a final time to the proper density and thickness. Self-supporting anodes and cathodes were used to assemble bipolar single cells using anode and cathode end plate hardware.

2.4. Special test fixture

The special test fixture in Fig. 1 was designed to evaluate lithium-ion cell components in a single cell bipolar configuration. Anode and cathode compositions were sprayed onto the 19 mm (0.75″) thick copper and aluminum end plates, respectively, during several spray/dry cycles, dried and compressed to final thickness.

The positive electrode (centered on the aluminum end plate in Fig. 1) was prepared for cell assembly by placing a Teflon O-ring in the end plate groove and centering the separator component over the cathode. The negative electrode (copper end plate) was bolted in position over the positive electrode with the proper cell gap provided by O-ring compression. The assembled cell was evacuated and back-filled with electrolyte from a syringe delivery system through the fillport in the negative electrode end plate.

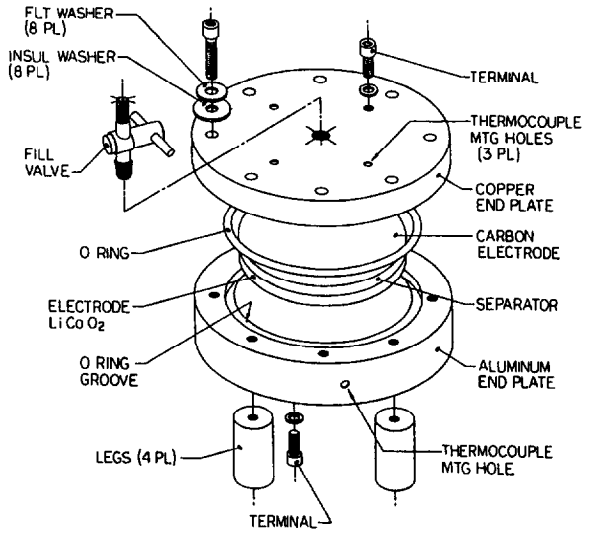

Fig. 1. Special test fixture for evaluation of lithium-ion single cells in bipolar configuration.

2.5. Bipolar plate and end plate fabrication

Multicell stacks were fabricated from 'bipolar hardware' consisting of bipolar plates and current collecting end plates. Bipolar plates were prepared by bonding a thermoplastic material such as high density polyethylene (HDPE), polypropylene (PPE) or Tefzel to a thin copper/aluminum bimetallic substrate. The procedure is illustrated in Fig. 2(a) and (b) for a 108 mm (4.25″) diameter bipolar plate using Tefzel thermoplastic material. Three Tefzel rings and a bimetallic substrate are properly aligned between the top and bottom capture mold sections so as to maintain a 3 mm ring/substrate overlap, Fig. 2(a). The two sections are bolted together and maintained under compression during the heating and cooling steps. After melting, the Tefzel components form an insulating ring, Fig. 2(b), of the proper height bonded to the periphery of the bimetallic substrate. Current collecting end plates are made in a similar manner. In that case, the negative electrode (anode) and positive electrode (cathode) substrates are 0.8 mm (0.032″) thick copper and aluminum disks, respectively. Of the three thermoplastic materials, Tefzel

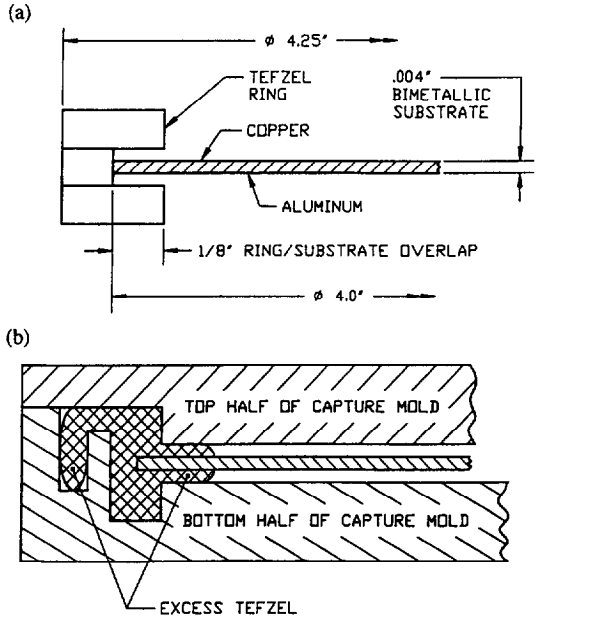

Fig. 2. (a) Tefzel/substrate sandwich prior to compression moulding. (b) Tefzel/substrate configuration after compression moulding.

forms the strongest bond with the copper/aluminum bimetallic substrate.

2.6. Multicell stack assembly

A multicell stack is assembled from bipolar plate and end plate hardware with sprayed-on electrode components. Each cell is provided with a layer of separator and the proper amount of electrolyte. The cell gap is established by compressing the stack of bipolar cells to final thickness, a value determined by the insulating ring thickness on the bipolar plate and end plate hardware. Stack compression is maintained by applying the proper amount of torque to the compression plate bolts. The insulation rings are sealed together using a hot gas welder to prevent electrolyte leakage between adjacent cells. A bipolar lithium-ion battery assembly is shown in Fig. 3.

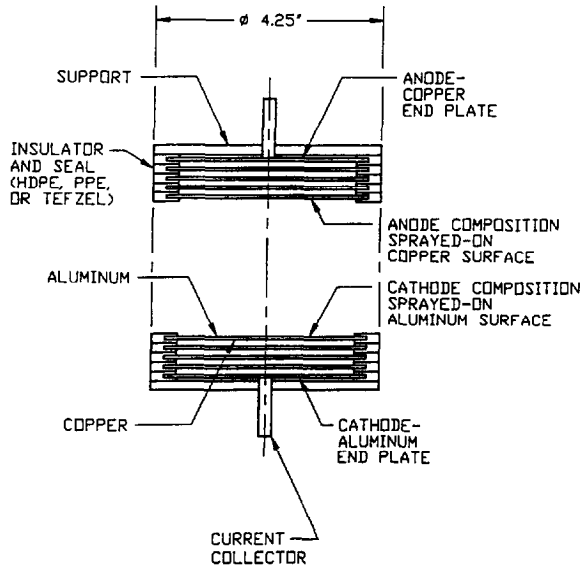

Fig. 3. Bipolar lithium-ion multicell battery assembly.

2.7. Single and multicell tests

All bipolar single cell tests were carried out with a Maccor 32-station cycler, computer programmed to control charge and discharge conditions and to store data. The multicell bipolar stack tests were conducted using test equipment custom designed by Yardney. Each cell or multicell stack was given a series of formation cycles prior to pulse discharge evaluation. During formation, a cell was charged at constant current to a maximum cell voltage, the end-of-charge-voltage (EOCV), after which taper charging continued (at the EOCV) for a total charge time or until a minimum current was reached. Each cell was kept on open circuit for 5 min after both charge and discharge. Discharge was carried out at constant current to the end-of discharge voltage (EODV) of 2.75 or 3.00.

3. Results and discussion

3.1. Electrolyte conductivity results

The conductivity of a 1 M $LiClO_4$ in 1:2 EC:DMC electrolyte was compared with three other electrolytes in Table 1 in order to find a replacement for the potentially unstable perchlorate ion. Both of the other more stable lithium salts, $LiPF_6$ and $LiAsF_6$, have higher conductivities than $LiClO_4$, in the mixed carbonate 1:2 EC:DMC, over the temperature range -20 to $+70$°C. The highest conductivity in Table 1 was observed with the 1 M $LiAsF_6$ in 1:2 EC:MF electrolyte in the temperature range -30 to $+40$°C. This electrolyte will be compared with the 1 M $LiClO_4$ and 1 M $LiPF_6$ mixed carbonate electrolytes in bipolar single cell tests.

3.2. Chemical compatibility test results

Lithiated nickel oxide was observed to have better chemical compatibility (less solubility) than either $LiCoO_2$ or

Table 1
Conductivity vs. temperature for 1 M $LiClO_4$, 1 M $LiPF_6$ and 1 M $LiAsF_6$ electrolytes

Temperature (°C)	Electrolyte conductivity (mS cm^{-1})			
	1 M $LiClO_4$ [a] 26 ppm H_2O	1 M $LiPF_6$ [a] 58 ppm H_2O	1 M $LiAsF_6$ [a] 29 ppm H_2O	1 M $LiAsF_6$ [b] 37 ppm H_2O
70	13.9	20.3	24.6	
60	13.9	20.3	19.7	
50	12.2	18.5	16.2	
40	11.0	16.2	14.5	22.6
30	9.86	14.5	12.7	20.8
20	8.41	12.4	9.2	17.9
10	6.96	10.0	7.83	14.5
0	5.66	7.8	6.96	13.9
−10	4.35	6.09	5.80	12.7
−20	0.98	freezes 2.46	freezes 2.61	10.7
−30	freezes			9.5

[a] Lithium salt dissolved in EC:DMC, 1:2 solvent mixture.
[b] Lithium salt dissolved in EC:MF, 1:2 solvent mixture.

Table 2
Chemical compatibility of $LiCoO_2$, $LiNiO_2$ and $LiMn_2O_4$ in EC-based 1 M $LiPF_6$ electrolytes after storage for a week at different temperatures

Mixture		25°C		40°C		60°C	
Oxide	Solvent [a]	Electrolyte color	Analysis for Co, Ni, Mn	Electrolyte color	Analysis for Co, Ni, Mn	Electrolyte color	Analysis for Co, Ni, Mn
$LiCoO_2$	EC:DEC	clear	0.0027% Co	purple	0.1230% Co	dark purple	0.33% Co
	EC:DMC		0.0010% Co	light purple	0.0017% Co		0.41% Co
	EC:DME	pale yellow	0.0013%Co	dark pink	0.3215% Co	dark pink	0.66% Co
$LiNiO_2$	EC:DEC	clear	0.0005% Ni	clear	0.0008% Ni	clear	no Ni
	EC:DMC		0.0006% Ni		0.0011% Ni		0.0009%
	EC:DME	pale yellow	0.0003% Ni		0.0001% Ni		no Ni
$LiMn_2O_4$	EC:DEC	pale yellow	0.0013% Mn	grey	0.0168% Mn	grey	0.053% Mn
	EC:DMC	yellow	0.0001% Mn		0.0034% Mn		0.13% Mn
	EC:DME		0.0025% Mn	pale yellow	0.0535% Mn	dark grey	0.40% Mn

[a] 1 M $LiPF_6$ electrolyte solvent mixture, 1:2 (vol./vol.).

Table 3
Chemical compatibility [a] of $LiCoO_2$, $LiNiO_2$ and $LiMn_2O_4$ with 1 M $LiAsF_6$ electrolyte [b] after storage for 1 week at different temperatures

Oxide type	25°C		40°C		60°C	
	Electrolyte color	Analysis for metal	Electrolyte color	Analysis for metal	Electrolyte color	Analysis for metal
$LiNiO_2$	pale pink	0.0005% Ni	pale yellow	0.0001% Ni	pale yellow	0.0013% Ni
$LiCoO_2$	pale yellow	0.0005% Co	pale pink	0.0001% Co	pale yellow	0.0012% Co
$LiMn_2O_4$	pale pink	0.0003% Mn	pink	0.0001% Mn	pale yellow	0.0009% Ni

[a] Each mixture consists of 10 g oxide mixed with 10 ml electrolyte and stored in a polypropylene bottle. A fresh mixture is used at each temperature.
[b] $LiAsF_6$ is dissolved in 1:2 (vol./vol.) EC:DMC mixed solvent.

Table 4
Chemical compatibility of $LiCoO_2$, $LiNiO_2$ and $LiMn_2O_4$ oxide materials with 1 M $LiPF_6$ and $LiAsF_6$ electrolytes after storage for 1 week at different temperatures

Sample mixture [a]		25°C		40°C	
Oxide	Electrolyte [b]	Electrolyte color	Analysis for metal	Electrolyte color	Analysis for metal
$LiCoO_2$	1 M $LiPF_6$	pale pink	0.0026% Co	clear	0.0007% Co
	1 M $LiAsF_6$	clear	0.0010% Co	brown	0.0662% Co
$LiNiO_2$	1 M $LiPF_6$	clear	0.0045% Ni	clear	0.0050% Ni
	1 M $LiAsF_6$	clear	0.0028% Ni	clear	0.0100% Ni
$LiMn_2O_4$	1 M $LiPF_6$	clear	0.0048% Mn	clear	0.0004% Mn
	1 M $LiASF_6$	clear	0.0003% Mn	yellowish-brown	0.1067% Mn

[a] Each sample mixture consists of 10 g oxide mixed with 10 ml electrolyte and stored in a polypropylene bottle. A fresh mixture is used at each temperature.
[b] Lithium salt is dissolved in 1:2 EC:MF.

$LiMn_2O_4$ at temperatures of 25, 40 and 60°C in 1 M $LiPF_6$ electrolytes prepared from three solvent mixtures, two carbonate/carbonate mixtures and a carbonate/ether combination. The results in Table 2 clearly indicate that $LiNiO_2$ is the least soluble of the three oxide materials over the above temperature range whereas $LiCoO_2$ and $LiMn_2O_4$ are quite soluble at 40 and 60°C, especially in the EC:DEC and EC:DME electrolytes. The three oxide materials were then examined for chemical compatibility in 1 M $LiAsF_6$ in 1:2 EC:DMC electrolyte. The results in Table 3 indicate that with the exception of Mn at 25°C and Ni at 60°C, substitution of the lithium salt $LiAsF_6$ for $LiPF_6$, drastically reduced the solubility of oxide material in the EC:DMC electrolyte, especially for both Mn and Co at 40 and 60°C. At 60°C, the electrolyte metal content was very low, with values of 0.0013, 0.0012 and 0.0009% for Ni, Co and Mn, respectively. Finally, each oxide was examined at temperatures of 25 and 40°C for chemical compatibility in 1 M $LiPF_6$ and 1 M $LiAsF_6$ electrolytes prepared from the 1:2 EC:MF solvent mixture. The results in Table 4 suggest that, of the two electrolytes, each oxide is relatively more stable (less soluble) in the 1 M $LiPF_4$ electrolyte. Comparison of the 1 M $LiAsF_6$ electrolytes in Tables 3 and 4 indicates that the solubility of each oxide material at 40°C increased by substitution of the MF solvent component in Table 4 for the DMC solvent component in Table 3. Also, comparison of the 1 M $LiPF_6$ electrolytes in Tables 2 and 4

suggests that the solubility of the Co and Mn oxide materials, although low to begin with, became lower by substitution of the MF solvent component in Table 4 for the DMC solvent component in Table 2, whereas the solubility of the Ni oxide material increased by a factor of four.

3.3. Bipolar single cell tests with special fixture

Figs. 4 and 5 show the voltage profile during the second cycle discharge for two bipolar single cells containing petroleum coke and graphite anodes, respectively. Both cells were charged to 4.0 V at a current density (CD) of 1.5 mA cm^{-2}. The cells were discharged to an EODV of 2.75 at a CD of 1.5 mA cm^{-2}. The cell with a petroleum coke anode delivered a capacity of 255 mAh g^{-1} of carbon with a sloping discharge voltage profile. As expected, the cell containing a graphite anode delivered higher capacity, 336 mAh g^{-1}, and had a much flatter discharge voltage profile.

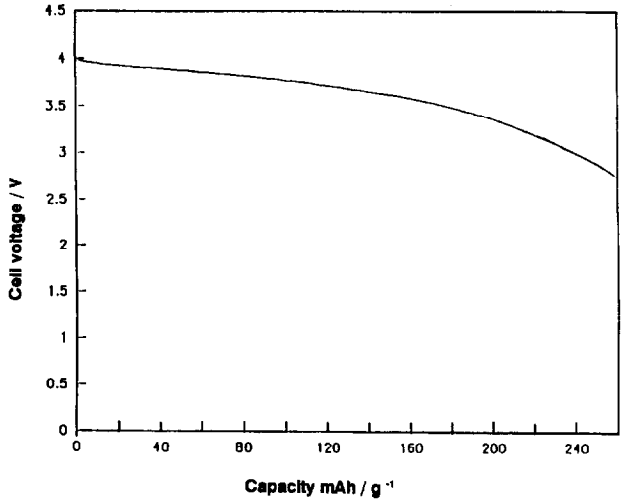

Fig. 4. Voltage profile during second discharge for cell containing petroleum coke anode, $LiCoO_2$ cathode, Celgard 2400 separator and 1 M $LiClO_4$ in 1:2 EC:DEC electrolyte. Charge to 4.0 V at CD of 1.5 mA cm^{-2}. Discharge at CD of 1.5 mA cm^{-2} to 2.75 V. Cell delivered a capacity of 255 mAh g^{-1} of anode carbon.

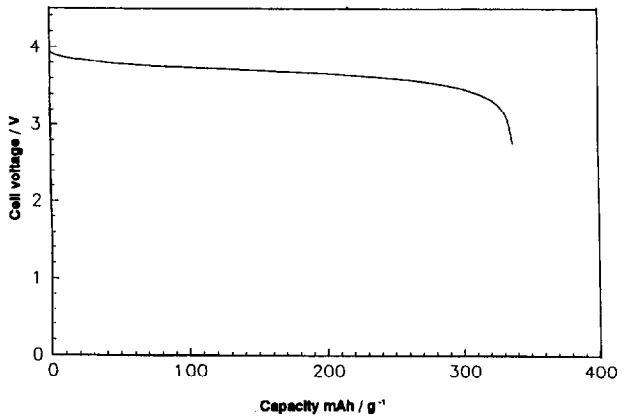

Fig. 5. Voltage profile during second discharge for cell containing graphite anode, $LiCoO_2$ cathode, Celgard 2400 separator and 1 M $LiClO_4$ in 1:2 EC:DMC electrolyte. Charge to 4.0 V at CD of 1.5 cm^{-2}. Discharge at CD of 1.5 mA cm^{-2} to 2.75 V. Cell delivered a capacity of 336 mAh g^{-1} of anode carbon.

A bipolar single cell with a graphite anode was charged at a current density of 2 mA cm^{-2} to 4.0 V and then continuously discharged and charged between the voltage limits of 2.5 and 4.1 for 3000 cycles. The cell was discharged at a CD of 42.1 mA cm^{-2} for 5 s and charged at a CD of 4.7 mA cm^{-2} for 45 s. The discharge/charge characteristics for this cell are shown in Fig. 6 for the last four cycles, 2997 through 3000. The end-of-pulse-voltage (EOPV) values versus cycle number are shown in Fig. 7.

After 3000 cycles, this cell was examined again for continuous discharge behavior. As shown in Fig. 8, the cell delivered a capacity of 334 mAh g^{-1} during discharge at a CD of 2 mA cm^{-2}, to an EODV value of 2.75, an indication that

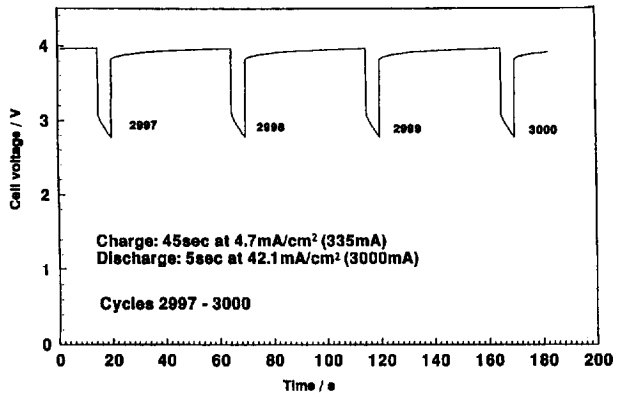

Fig. 6. Charge/discharge behavior of bipolar single cell during last four cycles, cycles 2997 through 3000. Cell contained graphite anode, $LiCoO_2$ cathode, Celgard 2400 separator and 1 M $LiClO_4$ in 1:2 EC:DMC electrolyte.

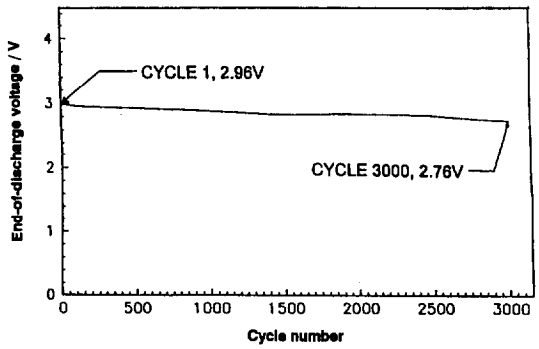

Fig. 7. EOPV values vs. cycle number for the bipolar lithium-ion single cell in Fig. 6.

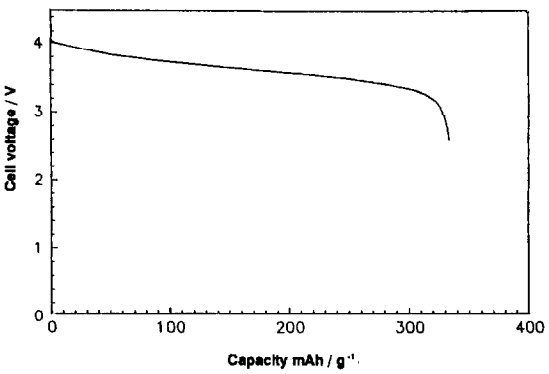

Fig. 8. Discharge behavior of bipolar lithium-ion single cell after 3000 charge/discharge cycles. Cell delivered 334 mAh g^{-1} at CD of 2 mA cm^{-2}.

Table 5
Anode capacity values during formation for two cells, each containing a graphite anode, $LiNiO_2$ cathode, Celgard 2500 separator and lithium perchlorate electrolyte

Cycle	Anode capacity (mAh g^{-1})	
	First cell	Second cell
1	389.9	308.8
2	391.5	323.9
3	385.0	326.1
4	388.0	330.9
5	387.3	325.5
6	379.9	324.8
7	381.5	323.5
8	378.5	324.6
9	368.3	322.6
10	367.4	320.0

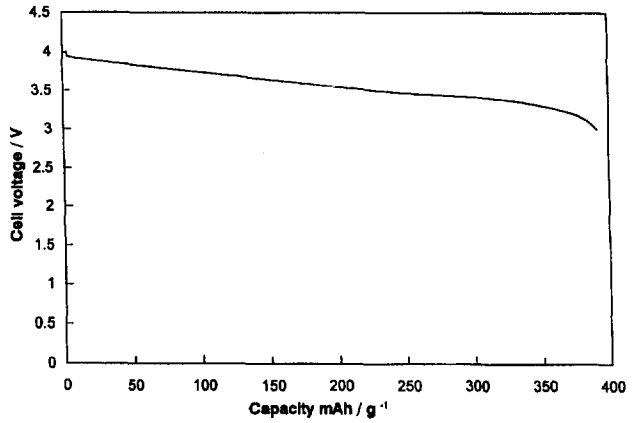

Fig. 9. Voltage profile during discharge step of cycle two for cell containing graphite anode, $LiCoO_2$ cathode, Celgard 2400 separator and 1 M $LiClO_4$ in 1:2 EC:DMC electrolyte. Cell delivered a capacity of 391.5 mAh g^{-1} of anode carbon.

the pulse discharge would not affect cell performance in a 100% DOD application.

Anode capacity values are shown in Table 5 for two cells during formation. Both cells contained a graphite anode, lithiated nickel oxide cathode, Celgard 2500 separator and 1 M $LiClO_4$ in 1:2 EC:DMC electrolyte. The first cell delivered a maximum capacity of 391.5 mAh g^{-1} during the discharge step of cycle two, as shown by the voltage profile in Fig. 9. However, this cell contained only 1.0 g of anode composition (0.9 g graphite), less than the 2 Ah capacity requirement on scale-up to a 280 mm (11 inch) diameter cell for the 270 V bipolar battery. The second cell was assembled with anode loading of 1.42 g, equivalent to the 2 Ah capacity requirement on scale-up. The maximum capacity for this cell in Table 5 was somewhat lower, 330.9 mAh g^{-1}, during formation cycle 4.

3.4. Bipolar single cell tests with endplate hardware

The $LiCoO_2$ cathode used in earlier cells was replaced with an $LiNiO_2$ cathode in four bipolar single cells assembled from end plate hardware, cells A, B, C and D. Cells A and B contained the 1 M $LiClO_4$ in 1:2 EC:DMC electrolyte. Cells C and D contained 1 M $LiPF_6$ in 1:2 EC:DMC and 1 M $LiAsF_6$ in 1:2 EC:MF electrolytes, respectively. All cells contained Celgard 2500 separator. These cells were charged at the 70 mA rate to 4.0 V, then taper charged for a total period of 10 h or until the charge current decreased to 20 mA. The cells were discharged at 70 mA to 3.0 V. Anode capacity values for these cells during formation are presented in Table 6.

The electrode fabrication method appears to have had the greatest effect on anode capacity during formation. The best result, 279 mAh g^{-1}, was obtained with cell A during cycle 7. This cell contained electrodes sprayed directly onto end plate hardware. For comparison, cells B, C and D contained self-supporting electrodes which were soaked with electrolyte prior to cell assembly. The best anode capacity value in Table 6 for each of these cells was 240 (cycle 10), 228 (cycle 7) and 236 mAh g^{-1} (cycles 3 and 4), respectively. Sprayed-on electrode components provide better electrode/end plate contact than self-supporting electrodes. These results illustrate the importance of minimizing contact resistance at the electrode/end plate interface.

The above cells were also pulse discharged at several current densities for selected compression plate torque values. The EOPV values are plotted versus current density in Fig. 10. Pulse parameters, torque values, pulse duration and EOPV values are presented in Table 7. Each cell, with one exception for cell A, was charged for a period of 45 s at one-ninth the discharge rate. The discharge period was for 5 s, or until cell voltage dropped below 2.5, or 2.0 in the case of cell A.

Electrolyte conductivity plays an important role during pulse discharge. For cell A, the EOPV value decreased dramatically at a pulse CD of 40 mA cm^{-2}, dropping below the

Table 6
Anode capacity values during formation of four bipolar single cells containing $LiNiO_2$ cathodes assembled from end plate hardware

Cycle	Cell A [a,b,c]	Cell B [b,d,g]	Cell C [d,e,g]	Cell D [d,f,g]
1	133	196	198	178
2	244	192	204	235
3	271	209	214	236
4	257	171	207	236
5	272	189	224	235
6	223	199	207	228
7	279	223	228	234
8	214	210	211	227
9	263	229	213	232
10	267	240	218	221

[a] Electrolyte compositions were sprayed onto end plate hardware.
[b] 1 M $LiClO_4$, 1:2 in EC:DMC.
[c] KS44 graphite.
[d] Self-supporting electrode components.
[e] 1 M $LiPF_6$, 1:2 in EC:DMC.
[f] 1 M $LiAsF_6$, 1:2 in EC:MF.
[g] KS15 graphite.

Table 7
Pulse parameters, compression plate torque, pulse duration and EOPV values for bipolar single cells A, B, C and D

Cell	Compression [a] torque (in. lb) [e]	Charge		Discharge			Cycle 100	
		I_c (mA)	Time (s)	I_d (mA)	CD (mA cm^{-2})	Time (s)	Time (s)	EOPV [c] (V)
		100	34	667	10	5	5	3.70
		151		1331	20			3.40
A	30	222	45	2000	30	5	5	2.99
		296		2662	40			1.97 [d]
B	40	85	45	643	10	5	5	3.299
		143		1286	20			2.691
C	30	60	45	527	10	5	5	3.573
		120		1054	20			3.218
		180		1581	30			2.858
		240		2108	40			2.510
	40	300		2635	50			2.612
	50	360		3162	60		4.967	2.484
D	30	60	45	527	10	5	5	3.672
		120		1054	20			3.415
		180		1581	30			3.157
		240		2108	40			2.932
		300		2635	50			2.686
	40	360		3162	60			2.509
	50	360		3162	60			2.606
	60	420		3689	70		4.761	2.486

[a] Cell components maintained under compression provided by torque on bolts holding compression plate together.
[b] Active area: Cell A, 65.5 cm^2; Cell B, 64.3 cm^2; Cells C and D, 52.7 cm^2.
[c] End-of-pulse-voltage (EOPV): cell voltage was set at 2.5 V during discharge.
[d] Cell A voltage was set at 2.0 V during discharge.
[e] Torque. One in. lb = 0.012 kg m.

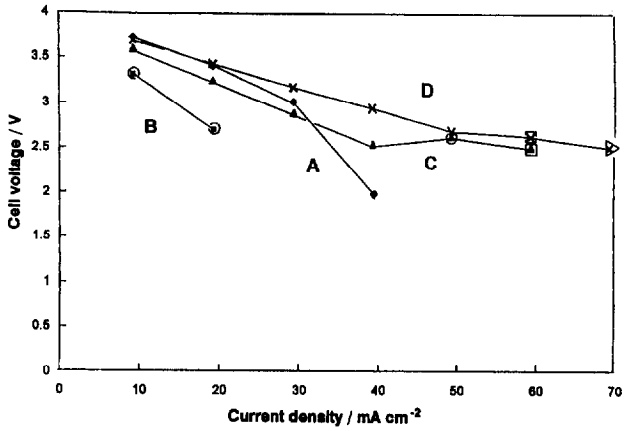

Fig. 10. Cell voltage vs. pulse current density for selected compression plate torque values. The EOPV value for cycle 100 is plotted for each current density. Minimum allowed EOPV was 2.0 V. Cell components are listed in Table 6. Initial torque was 30 in. lb, with the exception of cell A. Open circle: 40 in. lb; open square: 50 in. lb; open triangle: 60 in. lb. (1 in. lb = 0.012 kg m).

EOPV values for cells C and D, even though this cell achieved the highest anode capacity values during formation.

Based on the conductivity measurements in Table 1, cells C and D contained electrolytes with higher conductivity than the 1 M $LiClO_4$ electrolyte in cells A and B. Both cells C and D were pulse discharged successfully for 5 s at a CD of 60 mA cm^{-2}. The highest pulse CD, 70 mA cm^{-2}, was obtained for cell D which contained the 1 M $LiAsF_6$ in 1:2 EC:MF

Table 8
Anode capacity values during formation of two, four-cell stacks, each containing a graphite anode, $LiNiO_2$ cathode, Celgard 2500 separator and lithium perchlorate electrolyte

Cycle	Anode capacity (mAh g^{-1})	
	Stack A	Stack B
1	301	199
2	334	220
3	321	218
4	319	219
5	311	217
6	297	233
7	292	226
8	281	240
9	273	245
10	261	244

electrolyte, the electrolyte with the highest conductivity in the range −30 to +40°C.

3.5. Multicell stack tests

Two four-cell bipolar stacks, stacks A and B, were assembled from 108 mm (4.25 inch) diameter bipolar plate and end plate hardware with sprayed-on electrode components. Both stacks contained graphite anodes, $LiNiO_2$ cathodes, Celgard 2500 separators and I M $LiClO_4$ in 1:2 EC:DMC elec-

Table 9
Pulse parameters, pulse duration and EOPV values during cycle 100 for two, four-cell bipolar stacks

I (mA)	Pulse parameters				Cycle 100		
	Charge		Discharge			EOPV [a] (V)	
	Time (s)	I_d (mA)	CD (mA cm^{-2})	Time (s)	Time (s)	*A*	*B*
Stacks A and B 5 s pulse discharge							
100	34	667	10.2	5	5	14.48	14.9
151	45	1331	20.3	5	5	13.36	13.0
222	45	2000	30.5	5	5	12.34	11.0
296	45	2662	40.6	5	5	11.38	10.5
333	45	2998	45.7	5	4.86–5.02		9.95
371	45	3335	50.8	5	5	10.43	
Stack B 10 s pulse discharge							
167	40	667	10.2	10	10		13.6
333	40	1331	20.3	10	10		12.3
500	40	2000	30.5	10	10		10.9
583	40	2332	35.5	10	10		10.1

[a] End-of-pulse-voltage (EOPV): the stack voltage lower limit was set at 10 V during discharge.

trolyte. The stacks were charged at the rate to an EOCV of 16.0, then taper charged for a total period of 6 h or until the current decreased to 29 mA. The stacks were discharged at the 100 mA rate to 12.0 V. Anode capacity values for formation are listed in Table 8. The best anode capacity value was 334 (cycle 2) and 245 mAh g^{-1} (cycle 9) for stacks A and B, respectively.

Both stacks were pulse discharged for a period of 5 s at several current densities. In addition, stack B was pulse discharged for a period of 10 s at current densities in the range 10.2 to 35.5 mA cm^{-2}. Pulse parameters, pulse duration and EOPV values are presented in Table 9. Each stack was charged for a period of 45 s at one-ninth the discharge rate prior to the 5 s discharge period, with one exception for the 10 mA cm^{-2} discharge rate. Stack B was charged for a period of 40 s at one-fourth the discharge rate prior to the 10 s discharge period. The EOPV values obtained during cycle 100 for both the 5 and 10 s pulse discharge steps versus each CD value are plotted in Fig. 11. Stack A had the highest EOPV values at each CD, the largest being 50.8 mA cm^{-2}. For stack B, the EOPV values were somewhat lower than for stack A, with a maximum 5 s pulse CD value of 45.7 mA cm^{-2}. The lowest EOPV values were observed during the 10 s pulse discharge cycles of stack B. In this case, the maximum pulse CD value was 35.5 mA cm^{-2}. Voltage profile during the last six cycles for the stack A 5 s pulse discharge at a CD of 50.8 mA cm^{-2} and the stack B 10 s pulse discharge at a CD of 35.5 mA cm^{-2} are presented in Figs. 12 and 13, respectively.

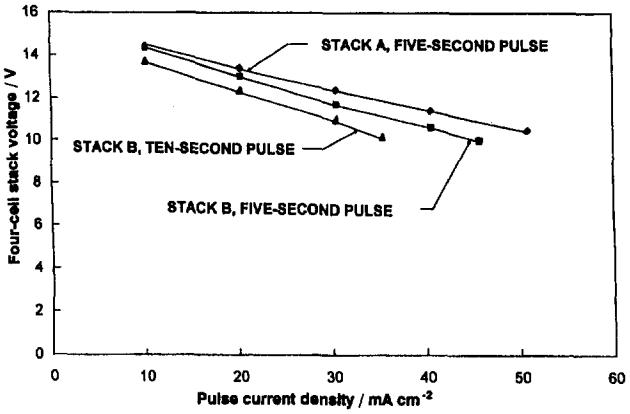

Fig. 11. Four-cell stack voltage vs. current density for pulse durations of 5 and 10 s. The EOPV value for cycle 100 is plotted for each current density. Minimum allowed EOPV was 10.0 V. Torque on the compression plate bolts was 30 in. lb (0.36 kg m).

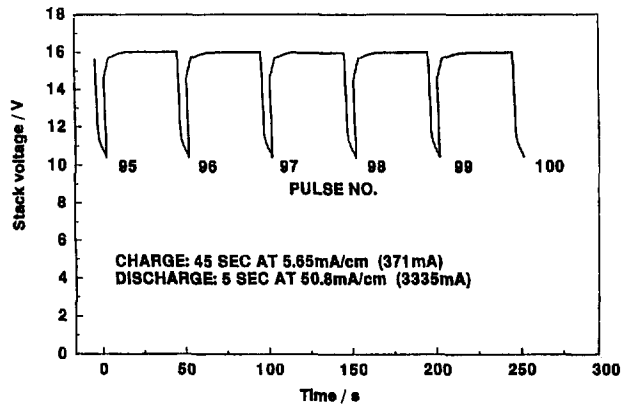

Fig. 12. Four-cell bipolar stack voltage profile during last six cycles of a 5 s pulse evaluation at a discharge current density of 50.8 mA cm^{-2}.

3.6. Initial design for a 270 V, 2 Ah bipolar lithium-ion battery

The initial design for a 270 V 2 Ah lithium-ion battery is presented in Table 10. Two columns of design parameter values are given: one for a 90-cell bipolar stack with 3.0 V per cell load voltage and the other for a 75-cell bipolar stack with a 3.6 V per cell load voltage. These designs are based on scale-up of the 108 mm (4.25″) diameter bipolar hardware

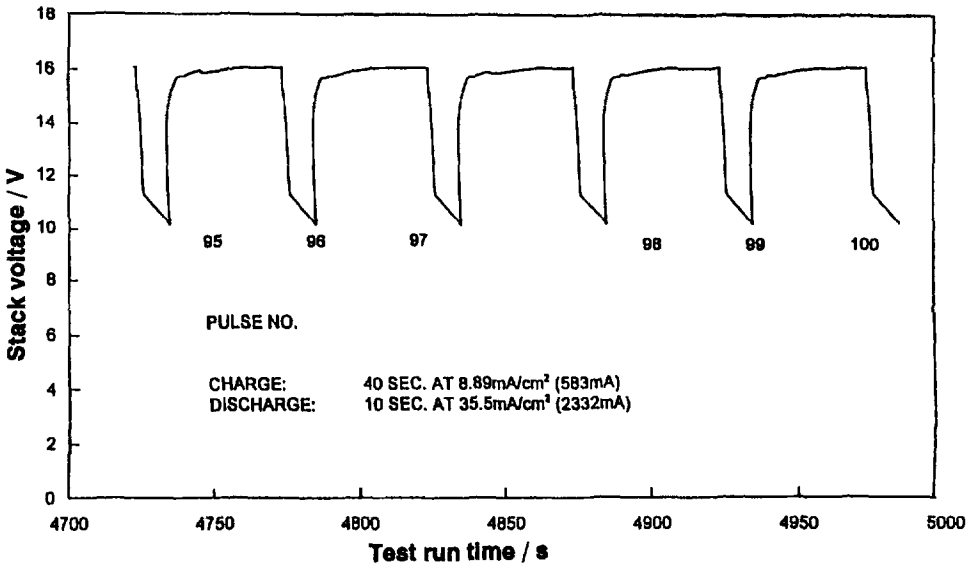

Fig. 13. Four-cell bipolar stack voltage profile during last six cycles of a 10 s pulse evaluation at a discharge current density of 35.5 mA cm^{-2}.

Table 10
Initial design specifications for 270 V, 2 Ah bipolar lithium-ion battery

Design parameter	Average load voltage per cell	
	3.0 V	3.6 V
Electrode diameter (in.)	10	10
Electrode diameter (mm)	254	254
Number of cells	90	75
Battery dimensions (in.) [a]	11.0 dia. × 1.50	11.0 dia. × 1.26
Battery dimensions (mm) [a]	280 dia. × 38	280 dia. × 32
Battery weight (kg)	6.69	5.62
Specific energy (Wh kg^{-1})	80.7	96.0
Energy density (Wh dm^{-3})	347	413
Specific power (kW kg^{-1}) [b]	1.19	1.18
Power density (kW dm^{-3}) [b]	5.12	5.08

[a] Does not include external battery case with support structure.
[b] Based on 5 s pulse discharge at CD of 70 mA cm^{-2} with average EOPV value of 2.50 V per cell.

results to 280 mm (11.0″) diameter bipolar plate and end plate hardware. The specific power and power density values are based on the 5 s pulse discharge results at a CD of 70 mA cm^{-2} with EOPV value of 2.5 V observed with a bipolar single cell containing a graphite anode assembled from end plate hardware. With the exception of the specific energy values, the energy density, specific power and power density values are much higher than for an equivalent prismatic design. Substitution of petroleum coke for the graphite anode should improve the rate capability/pulse duration period, and thus increase the specific power and power density parameter values.

4. Summary

Yardney Technical Products has successfully demonstrated the feasibility of using lithium-ion technology for high pulse-power applications in a bipolar configuration. A bipolar single cell assembled using the special test fixture was charged and pulse discharged for 3000 cycles. The CD was 42.1 mA cm^{-2} for each of the 5 s pulse discharge steps. The maximum pulse discharge CD, 70 mA cm^{-2}, was obtained with a graphite anode, lithiated nickel oxide cathode and 1 M $LiAsF_6$ in 1:2 EC:DMC electrolyte in a 108 mm (4.25″) diameter bipolar single cell assembled from end plate hardware. A four-cell bipolar stack assembled from 108 mm diameter bipolar plates and end plate hardware was pulse discharged for 5 s at a CD of 50.8 mA cm^{-2}, The EOPV was 10.43 during cycle 100. Initial designs have been developed for scale-up to 280 mm (11.0″) diameter, 270 V, 2 Ah bipolar lithium-ion batteries for pulse or continuous power applications.

Acknowledgements

The authors thank Sheila Danahey for fabrication of electrode components and assembly of bipolar cells and multicell stacks, and Fred Thompson and Ed Jackson for the design and construction of pulse test equipment for multicell stacks. This work was performed for Wright Laboratory under Contract No. F33615-91-C-2107.